



**HAL**  
open science

## Elasticity of particle-loaded liquid foams

F Gorlier, Yacine Khidas, Olivier Pitois

► **To cite this version:**

F Gorlier, Yacine Khidas, Olivier Pitois. Elasticity of particle-loaded liquid foams. *Soft Matter*, 2017, 13, pp.4533-4540 10.1039/C7SM00679A . hal-01559015

**HAL Id: hal-01559015**

**<https://hal.science/hal-01559015>**

Submitted on 10 Jul 2017

**HAL** is a multi-disciplinary open access archive for the deposit and dissemination of scientific research documents, whether they are published or not. The documents may come from teaching and research institutions in France or abroad, or from public or private research centers.

L'archive ouverte pluridisciplinaire **HAL**, est destinée au dépôt et à la diffusion de documents scientifiques de niveau recherche, publiés ou non, émanant des établissements d'enseignement et de recherche français ou étrangers, des laboratoires publics ou privés.

# Elasticity of particle-loaded liquid foams

F. Gorlier<sup>1</sup>, Y. Khidas<sup>2</sup> and O. Pitois<sup>1,\*</sup>

<sup>1</sup> *Université Paris Est, Laboratoire Navier, UMR 8205 CNRS – École des Ponts ParisTech – IFSTTAR  
cité Descartes, 2 allée Kepler, 77420 Champs-sur-Marne, France.*

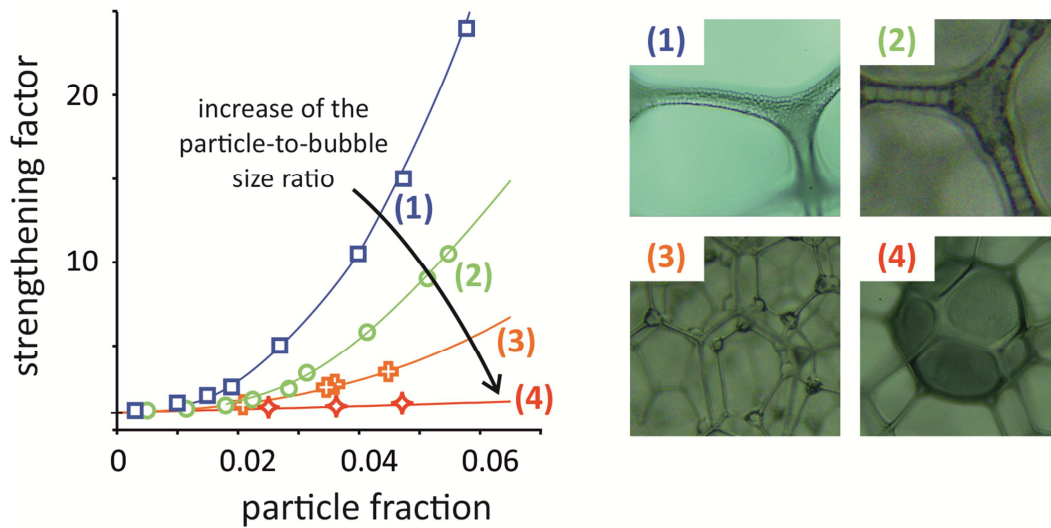
[francois.gorlier@ifsttar.fr](mailto:francois.gorlier@ifsttar.fr) ; [olivier.pitois@ifsttar.fr](mailto:olivier.pitois@ifsttar.fr)

<sup>2</sup> *Université Paris Est, Laboratoire Navier, UMR 8205 CNRS – École des Ponts ParisTech – IFSTTAR  
5 bd Descartes, 77454 Marne-la-Vallée Cedex 2, France.*

[yacine.khidas@u-pem.fr](mailto:yacine.khidas@u-pem.fr)

\* Corresponding author

Graphical abstract:



Abstract:

Mixing solid particles with liquid foam is a common process used in industry for manufacturing aerated materials. Desire for improvement of involved industrial processes and optimization of resulting foamed materials stimulates fundamental research on those complex mixtures of grains, bubbles and liquid. In this paper, we generate well-controlled particle-loaded liquid foams and we determine their elastic behavior as a function of particle size (6-3000  $\mu\text{m}$ ) and particle volume fraction (0-6%). We focus on both the elastic modulus exhibited by the material at small strain and the strain marking the end of the linear elastic regime. Results reveal the existence of a critical particle-to-bubble size ratio triggering a sharp transition between two well-defined regimes. For small size ratios, the behavior is governed by the mechanical properties of the solid grains, which have been proved to pack in the shape of a foam-embedded granular skeleton. In contrast, bubbles elasticity prevails in the second regime, where isolated large particles contribute only weakly to the rheological behavior of the foamed material. The modeling of elasticity for each regime allows for this transition to be normalized and compared with previously reported particle size-induced effects for foam drainage (Haffner et al. *J. Colloid Interface Sci.*, 2015, 458, 200–208) and solid foam mechanics (Khidas et al., *Compos. Sci. Technol.*, 2015, 119, 62–67). This highlights that rheology and the other properties of particle-loaded foams are subjected to the same size-induced morphological transition.

## Nomenclature

$\gamma$  liquid/gas surface tension

$D_b$  bubble diameter

$d_p$  particle diameter

$\phi_0$  gas volume fraction in the precursor foam

$\phi$  gas volume fraction in the foam sample

$\phi_{eq}$  average volume fraction value of the drained particle-free foam sample

$\phi_{p0}$  particle volume fraction in the particle/liquid suspension

$\phi_{p0}$  initial particle volume fraction in foam sample (before drainage)

$\phi_p$  particle volume fraction in drained foam sample

$\phi_c \approx 0.64$  volume fraction of packed spherical particles or bubbles

$\phi_p^*$  particle volume fraction marking the onset of foam strengthening, defined by a factor 2.5 on the modulus value with respect the reference particle-free foam

$\phi_p^{**}$  characteristic particle volume fraction introduced in order to construct a single curve

$$\epsilon_{crit}(\phi_p)/\epsilon_{crit}(0) = f(\phi_p/\phi_p^{**})$$

$G' \equiv G'(\phi, \phi_p, d_p/D_b)$  elastic modulus of particle-loaded foam

$G'_0 \equiv G'(\phi, \phi_p = 0)$  elastic modulus of particle-free foam

$G'_p$  elastic modulus of packed particles confined in the foam network (relevant for small particle-to-bubble size ratios)

$G'(\phi_p)$  elastic modulus of a continuous matrix (with elastic modulus  $G'_{matrix}$ ) loaded with hard solid particles

$\lambda$  confinement parameter defined as the ratio of the particle size and the characteristic size of the foam network

$\epsilon_{crit}$  critical strain amplitude (oscillatory rheometry) marking the end of the linear regime

## 1. Introduction

Mixing solid particles with liquid foam is a common process used in industry for manufacturing aerated materials. Typical examples can be found in the production of materials for the building industry<sup>1</sup>, of ceramic foams<sup>2</sup>, of products for the food<sup>3</sup> and cosmetic industries. Desire for improvement of both involved industrial processes and resulting foamed materials stimulates fundamental research, as evidenced by the recent literature on the subject<sup>4–23</sup>. Note also that the mining industry extensively resorts to mixtures of foam and particles through the flotation process that is widely used to separate ores<sup>24</sup>.

Previous studies were mainly focused on drainage and stability issues<sup>4–9,12–17,19,20</sup> because those two processes jeopardize fresh (not solidified) foamed materials. In contrast, only few studies have tackled rheological issues, for all types of foamed suspensions<sup>5,12,13,22,23,25–30</sup>. However, in the elaboration of optimized foamed materials, the rheological behavior of fresh complex foam is of

primary interest also. For example, elasticity and yield stress properties allow the material to sustain external forces and to keep its initial shape under gravity<sup>26,27,29</sup>. In contrast, filling of molds requires appropriate workability of the fresh foamy material. Two recent findings have considerably increased our knowledge on rheology of such foamy systems. Cohen-Addad et al.<sup>18</sup> have shown that adding a tiny amount of non-colloidal particles in aqueous foams can enhance the elastic and loss shear moduli by more than 1 order of magnitude. A particle-size dependence was reported, i.e., the effect is all the more pronounced as the particle size is smaller. Gorlier et al.<sup>22</sup> have investigated the effect of small particles, i.e., particle-to-bubble size ratio ( $d_p/D_b$ ) smaller than 0.1, and have highlighted a new elastic regime characterized by unequaled modulus values as well as independence on the size ratio. Gorlier et al. recognized that those two contradictory results are, however, not incompatible, insofar as the investigated ranges for  $d_p/D_b$  were different for those two studies. In the present study we investigate a range of  $d_p/D_b$  values covering both previously investigated ranges. As shown in the following, our results allow for a better understanding of those complex materials and suggest a simple physical picture for their elasticity.

## 2. Materials and methods

Particle-loaded foams are prepared by mixing aqueous foam and granular suspension.

### 2.1 Precursor foam

The first step of the preparation is the production of precursor aqueous foam with well-controlled bubble size  $D_b$  and gas volume fraction. Foaming liquid and perfluorohexane-saturated nitrogen are pushed through a T-junction allowing to control the bubble size by adjusting the flow rate of each fluid; for the present study only one bubble size has been used:  $D_b = 450\mu\text{m}$ . Produced bubbles are collected in a glass column and constant gas fraction over the foam column is set at 0.99 by imbibition from the top with foaming solution.

### 2.2 Granular suspensions

Secondarily, we prepare suspensions of polystyrene beads, with particle volume fraction chosen within the range 0.05-0.55 and a monodisperse particle size  $d_p \in [6, 10, 20, 30, 40, 80, 140, 500] \mu\text{m}$ . Note that foam and suspension share the same continuous phase, which is composed of distilled water 80% w/w and glycerol 20% w/w, and TTAB (trimethyl(tetradecyl)azanium bromide) at

a concentration  $5 \text{ g.L}^{-1}$ . Shear viscosity and density of that solution have been measured to be equal to  $1.7 \text{ mPa.s}$  and  $1050 \text{ kg.m}^{-3}$ , respectively. The surface tension of the solution has been measured to be equal to  $38 \text{ mN.m}^{-1}$ . The density of polystyrene beads is  $1050 \text{ kg.m}^{-3}$  so the latter are not subjected to sedimentation in the suspending liquid.

### *2.3. Foam/suspension Mixing*

Finally, the precursor foam and the granular suspension are mixed in a continuous process thanks to a mixing device based on the flow-focusing method<sup>15,17</sup>. By tuning the flow rates of both the foam and the suspension during the mixing step, the gas volume fraction  $\phi_0$  and the particle volume fraction  $\phi_{p0}$  can be tuned. Note also that bubble size is conserved during the mixing step, i.e.,  $D_b = 450\mu\text{m}$ . Resulting particle-loaded foams are continuously poured into the measurement cell (cup geometry: height = 7 cm and diameter = 37mm).

### *2.4. Preparation of the samples*

After this filling step, a six-bladed vane tool (height = 6 cm and diameter = 25mm) is inserted into the foam cell and the evolution of the sample is followed by measuring the shear elastic modulus through oscillatory rheometry (stress-controlled rheometer Malvern kinexus ultra+) with a strain of  $10^{-3}$  at 1Hz. After a transient regime, all samples were found to reach a constant value for the shear modulus. This behavior is attributed to the gravity drainage of the sample, during which both liquid and particles can flow down through the bubble assembly. It has been shown in a previous work<sup>17</sup> that this flow, as well as the final equilibrium state, i.e. the final gas fraction  $\phi$  and the final particle volume fraction  $\phi_p$ , are governed by the initial gas fraction  $\phi_0$ , the particle-to-bubble size ratio  $d_p/D_b$ , and the initial particle volume fraction within the interstitial suspension  $\varphi_{p0} = \phi_{p0}/(1 - \phi_0)$ . Therefore, for each particle size, a significant number of samples with different parameters  $\phi_0$  and  $\varphi_{p0}$  have been prepared in order to obtain drained samples with different parameters  $\phi$  and  $\phi_p$ . Note that due to limitations of the generation method we were not able to produce the most concentrated systems for all the particle sizes. Parameters  $\phi$  and  $\phi_p$  are measured thanks to a second cell (height = 7 cm and diameter = 26mm) also filled during the generation step. The bottom of this cell is a piston allowing for the particle-loaded foam to be partially pushed out after drainage. This setup allows sampling the foam along its height and the particle fraction profile is measured as follows: each sampled volume is first weighed and then rinsed several times with ethanol in order to break the foam and to remove glycerol (each time

centrifugation is performed for separating the particles from the liquid). Finally, the collected particle/ethanol mixture is let for drying (twelve hours at 60°C) and the resulting dried particles are weighed. For all the particle sizes, vertical profiles for particle volume fraction showed very good homogeneity of the samples for high particle loadings, i.e.  $\langle \phi_p \rangle \geq 0.02$  (see Gorlier et al.<sup>22</sup> for further details). For  $\langle \phi_p \rangle \leq 0.01$ , very good homogeneity was obtained for the large particle sizes, i.e.  $d_p \geq 40 \mu\text{m}$ , and samples with smaller particle sizes showed reasonable homogeneity, i.e.  $0.7 \leq \Delta\phi_p / \langle \phi_p \rangle \leq 1.3$ . Such a behavior can be explained by the effect of initial particle concentration on drainage<sup>17</sup>. For high concentration, particles are trapped by collective jamming, i.e., channel size is larger than particle size. This situation promotes uniform concentration profile. For low concentration, collective jamming is rather ineffective and particle trapping is mainly due to individual captures, i.e., channel size is equal to particle size. For such cases, the quantity of trapped particles is strongly related to channel size at equilibrium, which is known to increase near the bottom: capture is less effective in those areas.

### 2.5. Case of large particles

In order to investigate systems characterized by larger particle-to-bubble size ratio, we turn to another approach for making foams loaded with glass particles of diameter  $d_p = 3200 \mu\text{m}$ . Note that this size represents almost 10 bubbles. Precursor foam is continuously poured into the rheometry cell and the dry particles are spread by hand during the filling process, ensuring homogeneity as far as possible. Note that (i) the significant yield stress of the precursor foam ( $\approx 15 \text{ Pa}$ ) prevented particle settling; (ii) the elastic modulus of the precursor foam will be used as the reference elastic modulus for nondimensionalization purpose. We focused on systems with particle volume fractions equal to 0.025 and 0.05.

### 2.6. Rheometry

After the drainage step, the rheology measurement procedure starts: elastic and loss moduli are measured as a function of shear strain amplitude  $\epsilon$  at a fixed frequency of 1Hz, from  $\epsilon = 10^{-4}$  to  $\epsilon = 10$ . The critical strain amplitude  $\epsilon_{crit}$  marking the end of the linear regime is determined using the following criterium:  $G'(\epsilon_{crit}) = 0.98G'(\epsilon \rightarrow 0)$ . For several strongly loaded systems, reaching the linear regime required to decrease more the strain amplitude, which induced significant noise on  $G'$  and inaccuracy on  $\epsilon_{crit}$ . Note that (i) to avoid slippage on the cell wall as the shear stress is applied, the cell surface has been striated to jam the bubbles; (ii) the minimal gap in the vane-cup

geometry represents 12 bubble diameters; (iii) the presence of perfluorohexane inside bubbles strongly reduces the foam ripening rate<sup>31</sup> which allows aging effects to be ignored over the time scale of measurements.

### 3. Results

Results showing the effect of particle size on foam rheology are presented in figure 1. For given particle volume fraction, both elastic and loss moduli increase as particle size decreases, and for the largest investigated particle sizes, the moduli are very close to those obtained for particle-free foams. The effect of particle loading is all the more significant as the strain amplitude is smaller. Note also that the critical strain amplitude  $\epsilon_{crit}$  marking the end of the linear elastic regime decreases as particle size decreases. For significant particle loadings and small particles, for example  $\phi_p = 0.045$  and  $d_p \leq 40 \mu\text{m}$ , the linear regime is reached for  $\epsilon_{crit} < 10^{-3}$ . In contrast for the largest particle sizes  $\epsilon_{crit} \sim 10^{-1}$ , as for particle-free foams.

Results obtained for  $G' \equiv G'(\epsilon \rightarrow 0)$  are plotted in figure 2a as a function of  $\phi_p$  for all the investigated particle sizes. Note that modulus values are divided by the modulus of the corresponding particle-free foam, i.e. the aqueous foam with same bubble size and gas volume fraction, as estimated by the following relationship<sup>32</sup>:  $G'_0 \equiv G'(\phi, 0) \approx b(\gamma/D_b)\phi(\phi - \phi_c)$ . As we measured  $G' = 44 \text{ Pa}$  for the drained particle-free foam, which is characterized by  $\phi = \phi_{eq} \approx 0.97$ , chosen parameters are  $b \approx 1.8$  and  $\phi_c \approx 0.64$ , the volume fraction corresponding to the random close packing of spheres. For particle volume fractions  $\phi_p \gtrsim 0.02$ , elastic moduli show a strong evolution from the low values, measured for the largest particle sizes, towards the high values measured for the small particle sizes. For  $\phi_p \approx 0.05$ , more than one order of magnitude is measured between the smallest and the largest modulus values. The size-induced evolution is presented in figure 2b, revealing a transition-like behavior for all particle volume fractions: (i) the modulus does not evolve significantly for small particle-to-bubble size ratios, i.e., for  $d_p/D_b \lesssim 0.03$ , (ii) it decreases strongly for  $0.03 \leq d_p/D_b \lesssim 0.2$ , (iii) it remains close to unity for  $d_p/D_b \gtrsim 0.2$ .

Critical strain amplitudes  $\epsilon_{crit}$  are reported in figure 3a as a function of particle volume fraction. At small particle volume fractions the critical strain of loaded foams is equal to the critical strain of particle-free foams, i.e.,  $\epsilon_{crit}(\phi_p) \approx \epsilon_{crit}(0)$ . However, as  $\phi_p$  increases,  $\epsilon_{crit}(\phi_p)$  decreases over two orders of magnitude. Note that the  $\phi_p$  value for which  $\epsilon_{crit}(\phi_p)$  starts to decrease is itself smaller as  $d_p$  is smaller.

Images of the foam microstructure are presented in figure 4, revealing the organization of particles for similar particle loadings. For small particle-to-bubble size ratios, the particles aggregate in the interstitial foam network (Fig. 4a,b). Note that particles can form packings (Fig. 4a) or strings (Fig. 4b). For those size ratios, particles form a granular skeleton. For larger size ratios, particles are located in the nodes of the network without forming a percolating structure (Fig. 4c). Finally, the microstructure for the largest investigated size ratio is made of isolated large particles embedded in aqueous foam (Fig. 4d).

#### 4. Discussion

Our results confirm that particle size has strong influence on the rheology of particle-loaded foams. The shear elastic modulus measured at small strain amplitude shows a transition-like behavior as a function of particle size.

##### 4.1. Case of small size ratios

In a previous paper<sup>22</sup>, it has been shown that modulus values obtained for small particle-to-bubble size ratios can be described by a simple model accounting for the intrinsic elasticity of the interstitial skeleton made of packed particles. The contribution of the skeleton is assumed to be given by  $G_s \approx aG_p(1 - \phi)^2$ , where  $G_p$  is the bulk shear modulus of the matrix forming the skeleton and  $a$  is a numerical coefficient<sup>33</sup>. This contribution superimposes to that of the bubble assembly  $G'_0 \approx b(\gamma/D_b)\phi(\phi - \phi_c)$ , and the global elastic behavior is obtained by summing those two contributions:  $G' \approx aG_p(1 - \phi)^2 + b(\gamma/D_b)\phi(\phi - \phi_c)$ . As the skeleton is made of packed particles, the volume fraction occupied by the skeleton is  $1 - \phi \approx \phi_p/\phi_c$ , and the reduced elastic modulus can be written:

$$g_1 \equiv \frac{G'(\phi, \phi_p, a_p/D_b \ll 1)}{G'_0} = 1 + \left(\frac{a}{b}\right) \frac{G_0}{\gamma/D_b} h(\phi_p) \quad (\text{eq. 1})$$

where  $h(\phi_p) = [(\phi_c/\phi_p - 1)(\phi_c/\phi_p - 1 - \phi_c^2/\phi_p)]^{-1}$ . According to literature<sup>32,33</sup>, we set  $a/b = 0.36$ . Therefore,  $G_p$  is the only fitting parameter and it represents the shear elastic modulus of the bulk granular packing forming the skeleton. As shown in figure 2a, good agreement is obtained with our data over the full range of  $\phi_p$  values as  $G_p = 150$  kPa is used in eq. 1. This value has been found to be compatible with the elastic modulus measured for bulk granular material under

confinement pressures corresponding to pressures exerted by the bubbles on the granular skeleton<sup>22</sup> in foam.

#### 4.2. Case of large size ratios

In contrast, for systems characterized by the largest investigated size ratio, i.e.  $d_p/D_b \gtrsim 1$ , particles do not form such a granular structure. Instead, isolated large particles are embedded in aqueous foam, which is known as yield stress fluid<sup>34,35</sup>. It is therefore natural to describe such particle-loaded material with the modeling proposed for suspensions of non-colloidal particles in yield stress fluids<sup>36</sup>. The strengthening effect due to solid particles embedded in continuous matrix of elastic modulus  $G'_{matrix}$  has been shown to be given by:  $G'(\phi_p)/G'_{matrix} = (1 - \phi_p/\phi_c)^{-2.5\phi_c}$ . Applying this result to our system requires to express the bulk elastic modulus  $G'_{matrix}$  of the embedding foam. Within our experimental configuration, the average volume fraction value of the drained particle-free foam, that fills spaces between large particle inclusions, is  $\phi_{eq}$ . This value differs from the value  $\phi$  measured for the particle-loaded foam, i.e.,  $\phi = \phi_{eq}(1 - \phi_p)$ , so the modulus of the reference aqueous foam  $G'_0 = b(\gamma/D_b)\phi(\phi - \phi_c)$  differs from the modulus of the embedding foam  $G'_{matrix} = b(\gamma/D_b)\phi_{eq}(\phi_{eq} - \phi_c)$ . Therefore, we introduce the factor  $k(\phi_p) = G'_{matrix}/G'_0$ , which can be written  $k(\phi_p) = (\phi_{eq} - \phi_c)/[(1 - \phi_p)(\phi_{eq}(1 - \phi_p) - \phi_c)]$ . Within our experimental configuration,  $k(\phi_p)$  varies from 1 to 1.23 as  $\phi_p$  increases from 0 to 0.05. Note that other experimental configurations are expected to induce other behaviors for  $k(\phi_p)$ : in Cohen-Addad et al.<sup>18</sup> for example, particle-loaded foams were obtained by mixing the reference foam with dry particles and the system was not expected to drain, i.e., in such a case, the embedding foam is always the reference foam and  $k(\phi_p) = 1$ .

The reduced shear elastic modulus is obtained by writing<sup>37</sup>  $G'(\phi, \phi_p, d_p/D_b \gg 1)/G'_0 = G'(\phi_p)/G'_{matrix} \times G'_{matrix}/G'_0$ , which can be expressed as:

$$g_0 \equiv \frac{G'(\phi, \phi_p, d_p/D_b \gg 1)}{G'_0} = k(\phi_p) \times \left(1 - \frac{\phi_p}{\phi_c}\right)^{-2.5\phi_c} \quad (\text{eq. 2})$$

The particle-to-bubble size ratio does not appear in eq. 2 because foam is assumed to behave as a continuous material. Eq. 2 is plotted in Fig. 2a, using  $k(\phi_p) = (\phi_{eq} - \phi_c)/[(1 - \phi_p)(\phi_{eq}(1 - \phi_p) - \phi_c)]$ , and it is shown to compare well with data obtained for  $d_p/D_b \gtrsim 1$ .

### 4.3. Case of intermediate size ratios

#### 4.3.1. Transition behavior of the elastic modulus

The elastic modulus of particle-loaded foams appears to evolve from the upper bound given by eq. 1 and valid for  $d_p/D_b \ll 1$ , towards the lower bound given by eq. 2 and valid for  $d_p/D_b \gg 1$ . In order to highlight the transition behavior over the whole range of particle volume fractions, we introduce the normalized elastic modulus:

$$\tilde{G}' = \frac{\frac{G'(\phi, \phi_p, d_p/D_b)}{G_0} g_0}{g_1 - g_0} \quad (\text{eq. 3})$$

In eq. 3,  $\tilde{G}'$  measures the magnitude of  $G'(\phi, \phi_p, d_p/D_b)$  with respect to both upper and lower bounds defined by eqs 1 and 2, for which  $\tilde{G}' = 1$  and  $\tilde{G}' = 0$  respectively.  $\tilde{G}'$  is plotted in figure 5a as a function of  $d_p/D_b$ , for several  $\phi_p$  values and using  $G_p = 150$  kPa<sup>22</sup>. It is shown that for all  $\phi_p$  values  $\tilde{G}'$  decreases from 1 over two orders of magnitude as  $d_p/D_b$  increases from 0.01 to 1. Note that the decrease is not observed from the smallest  $d_p/D_b$  values, for which  $\tilde{G}' \approx 1$ . In the inset of figure 5a,  $\tilde{G}'$  is plotted as a function of the so-called *confinement parameter*,  $\lambda$ . This parameter, introduced by Louvet et al.<sup>38</sup> in order to describe the capture of particles within interstitial foam networks, compares the size of particles to the size of constrictions formed between contacting bubbles in foam:  $\lambda = C(\phi) d_p/D_b$ , with  $C(\phi) = (1 + 0.57(1 - \phi)^{0.27}) / (0.27\sqrt{(1 - \phi)} + 3.17(1 - \phi)^{2.75})$ . We choose to use  $\phi = \phi_{eq} \approx 0.97$ , the average value of the gas volume fraction in the drained particle-free foam. As shown in Fig. 5a, the transition between the regime  $\tilde{G}' \approx 1$  and the regime of decrease occurs at  $\lambda \approx 1$ . Note that as  $\lambda$  increases from  $\lambda \approx 1$ , the deformation of interfaces delimiting the foam network intensifies and simultaneously particles increase their contact surface area with the liquid/gas interface<sup>16</sup>, which can be viewed as the progressive exclusion of the particles from the bulk foam network. For foam drainage and as well as for mechanics of solid foams, this size-induced morphological evolution, also named *particle exclusion transition*, has been found to induce a significant evolution of the foam properties<sup>17,37</sup>. Therefore, figure 5a shows that rheology of particle-loaded foams also is governed by this morphological transition.

### 4.3.2. Consistency with previous work

Now, we show how results from Cohen-Addad et al.<sup>18</sup> can be interpreted within the framework of the *particle exclusion transition* by plotting  $\tilde{G}'$  as a function of  $d_p/D_b$  or  $\lambda$ . The starting point is to determine the optimal elastic modulus which characterizes the system for  $\lambda \lesssim 1$ , even though this modulus has not been measured by Cohen-Addad et al.<sup>18</sup>. This can be done by choosing a  $\phi_p$  value<sup>i</sup> and adjusting  $G_p$  in eq. 3 in order to get a consistent plot with our data. The resulting plot is presented in figure 5b. We would like to stress three issues: (i) despite differences in bubble and particle sizes, previous results are found to complement our data and to exhibit the same behavior in terms of power law, i.e.  $\tilde{G}' \sim (d_p/D_b)^{-1.5}$ ; (ii) previous results corresponding to plate-like particles are clearly shown to not belong to the same set of data as spherical particles; (iii) the value obtained for  $G_p$  is equal to 1.5 MPa. This value is significantly larger than the one obtained for our data (0.15 MPa), but in fact it is in perfect agreement with the expected value for the bulk granular material<sup>22</sup>. As already mentioned in Gorlier et al.<sup>22</sup>, we stress that within our experimental conditions the confinement pressure, i.e., the pressure exerted by liquid/gas interface on packed particles, is rather low and it does not allow reaching the full range of values expected for  $G_p$ . In contrast, the confinement pressure involved in the experiment of Cohen-Addad et al. is significantly larger<sup>ii</sup> and the elasticity of the granular skeleton is therefore expected to be in much closer agreement with measured elastic modulus of bulk granular matter.

### 4.3.3. Transition regime expressed in terms of particle volume fraction

Previous work<sup>18</sup> interpreted the particle size-induced evolution for foam elasticity in terms of particle volume fraction for rigidity percolation threshold. We consider this approach also and we determine the particle volume fraction  $\phi_p^*$  marking the onset of particle-induced strengthening. Firstly, we focus on the smallest particles, characterized by  $\lambda < 1$ . For such a situation, strengthening is expected to start as packed particles fully fill the interstitial network, i.e.  $\phi_p^* \approx \phi_c(1 - \phi_{eq}) \approx 0.015$ , where  $\phi_{eq}$  is the average gas volume fraction of the reference particle-free foam. For such a  $\phi_p^*$  value, the modulus of foams containing particles with diameter  $d_p \leq 20 \mu\text{m}$  is increased by

---

<sup>i</sup> We choose particle volume fraction as large as possible with our data, i.e.  $\phi_p \approx 0.07$ , in order to observe the maximum strengthening effect.

<sup>ii</sup> Parameters of aqueous foams used by Cohen-Addad et al. are:  $D_b = 30 \mu\text{m}$ ,  $\phi \approx 0.9$ . The osmotic pressure is expected to be  $\Pi = 1.2 \gamma/D_b \approx 1600 \text{ Pa}$ , which is 4 times larger than the confinement pressure in our experiment.

a factor 2.5 (see Fig. 2a). Then, for all other particle sizes, we determine  $\phi_p^*$  such that  $G'(\phi_p^*)/G'_{matrix} \approx 2.5$ , and we follow the same procedure for data from Cohen-Addad et al. The two sets of  $\phi_p^*$  values are plotted in figure 6 as a function of  $d_p/D_b$ , showing a transition in the  $\phi_p^*$  values, from  $\phi_p^* \approx \phi_c(1 - \phi_{eq})$  for small size ratios, towards  $\phi_p^* \approx 0.3$ . The latter corresponds to the expected value for large size ratios deduced from eq. 2 with  $k(\phi_p) = 1$  (i.e., corresponding to the experimental conditions of Cohen-Addad et al.):  $\phi_p^* \approx \phi_c(1 - (2.5)^{-1/(2.5\phi_c)})$ . Therefore, expressing the onset of foam strengthening in terms of particle volume fraction highlights also the so-called *particle exclusion transition* between two extreme configurations: for  $\lambda < 1$  the particles concentrate into the interstitial foam network, whereas for  $\lambda \gg 1$  the particles are large inclusions embedded into aqueous foam. Although those two bounds have been identified, the global modeling of the transition is still lacking. It is however possible to bring some understanding elements for the behavior observed at small particle-to-bubble size ratios. Indeed, a particular morphological configuration has been identified in figure 4c: particles concentrate into the foam network in forming particle strings along the Plateau borders. One can estimate the corresponding particle volume fraction  $\phi_p^{string}$  as follows. First, we assume the Kelvin cell geometry<sup>32</sup>, i.e. 6 nodes (each with 2 half-Plateau borders) per gas bubble of volume  $\Omega_g = \pi D_b^3/6$ , and a node-to-node distance  $L_{nn} \approx 0.36D_b$ . Therefore, the number of particles per bubble is  $6(2L_{nn}/d_p - 1)$ , where the constant (-1) accounts for the non-overlapping of node-to-node distances. Combining those expressions gives the volume of particles per bubble:  $\Omega_p \approx (0.72D_b/d_p - 1)\pi d_p^3$ . The latter can be used to estimate the corresponding volume of interstitial phase, i.e. liquid plus particles, per bubble:  $\Omega_i \approx (1/\varphi_1)(0.72D_b/d_p - 1)\pi d_p^3$ , where  $\varphi_1 \approx 1/3$  is the particle volume fraction within the interstitial phase for the particle-string configuration (see details in Haffner et al.<sup>14</sup>). The particle volume fraction in the particle-string configuration is  $\phi_p^{string} \approx \Omega_p/(\Omega_i + \Omega_g)$ , which can be expressed as:

$$\phi_p^{string} \approx \left( 3 + \frac{D_b^3}{6(0.72D_b/d_p - 1)d_p^3} \right)^{-1} \quad (\text{eq. 4})$$

Eq. 4 is expected to apply as particles are too big for forming a 3D packing structure into the foam network, but small enough for percolating through that network. As shown in the inset of figure 6, eq. 4 predicts correctly the strong increase observed for  $\phi_p^*$  as  $\lambda \approx 2$ . From that value, increasing the confinement parameter results in progressive particles exclusion from the interstitial network.

#### 4.3.4. Transition regime expressed in terms of critical strain amplitude

Finally, we turn to results for the critical strain amplitudes (Fig. 3a), which have been found to depend on both particle size and particle volume fraction. Similarly to the procedure applied to  $G'$ , we introduce the characteristic particle volume fraction  $\phi_p^{**}$  in order to construct a single curve  $\epsilon_{crit}(\phi_p)/\epsilon_{crit}(0) = f(\phi_p/\phi_p^{**})$  for all the particle sizes (see figure 3b). The values  $\phi_p^{**}$  are plotted as a function of  $\lambda$  in the inset of figure 3b. It is shown that  $\phi_p^{**}$  exhibits the same behavior as  $\phi_p^*$ , i.e.,  $\phi_p^{**} \approx \phi_c(1 - \phi_{eq}) \approx 0.15$  for  $\lambda \lesssim 1$  and  $\phi_p^{**} \approx \phi_p^{string}$  for  $1.5 \lesssim \lambda \lesssim 3$ , showing that within that range of size ratios,  $G'$  and  $\epsilon_{crit}$  are both governed by the mechanical properties of packing structures formed by particles in the interstitial foam network.

## 5. Conclusion

We have generated well-controlled particle-loaded liquid foams and we have measured both the elastic modulus exhibited by the material at small strain and the strain marking the end of the linear elastic regime. Results have revealed the existence of a critical particle-to-bubble size ratio triggering a sharp transition between two well-defined regimes, which have been found to be equivalently described in terms of elastic modulus or in terms of particle volume fraction for the onset of strengthening. Previous results from literature have been successfully incorporated to our description, providing a consistent set of data supporting the physical picture of a transition between two regimes. For small size ratios, more precisely as the confinement parameter  $\lambda$  is smaller than unity, the behavior is governed by the mechanical properties of the solid grains, which have been proved to pack in the shape of a foam-embedded granular skeleton. The elasticity of the granular skeleton has been estimated using models available for solid foams, to which elasticity of the bubble assembly has been added. In contrast, bubbles elasticity prevails in the second regime, where isolated large particles contribute only weakly to the rheological behavior of the foamed material. The general modeling available for non-colloidal hard particles embedded in soft elastic matrix has been shown to describe correctly the results in the second regime. Both theoretical bounds, for small and large particles, have been used to normalize the observed transition, highlighting the strong analogy with previously reported particle size-induced effects on foam drainage<sup>17</sup> and solid foam mechanics<sup>37</sup>. In particular, the normalized elastic modulus has been shown to decrease as a function of the particle-to-bubble size ratio according to a power law  $\tilde{G}' \sim (d_p/D_b)^{-n}$ , with  $n$  close to 1.5. This indicates that rheology and the other properties of particle-loaded foams are subjected to the same size-induced morphological transition. Further work could be devoted to the modeling of the *particle exclusion transition*.

## Acknowledgements

We thank D. Hautemayou and C. Mézière for technical support. We gratefully acknowledge financial support from Agence Nationale de la Recherche (Grant No. ANR-13-RMNP-0003-01) and French Space Agency (convention CNES/70980). We thank X. Chateau and G. Ovarlez for fruitful discussions.

## References

- 1 R. K. Dhir, M. D. Newlands and A. McCarthy, Eds., *Use of Foamed Concrete in Construction*, Thomas Telford Ltd, London, 2005.
- 2 A. R. Studart, U. T. Gonzenbach, E. Tervoort and L. J. Gauckler, *Journal of the American Ceramic Society*, 2006, **89**, 1771–1789.
- 3 A. Wilson, Ed., *Foams: Physics, Chemistry and Structure*, Springer London, London, 1989.
- 4 A. M. Sani and K. K. Mohanty, *Colloids and Surfaces A: Physicochemical and Engineering Aspects*, 2009, **340**, 174–181.
- 5 R. Guillermic, A. Salonen, J. Emile and A. Saint-Jalmes, *Soft Matter*, 2009, **5**, 4975–4982.
- 6 A. Britan, M. Liverts, G. Ben-Dor, S. A. Koehler and N. Bennani, *Colloids and Surfaces A: Physicochemical and Engineering Aspects*, 2009, **344**, 15–23.
- 7 F. Carn, A. Colin, O. Pitois, M. Vignes-Adler and R. Backov, *Langmuir*, 2009, **25**, 7847–7856.
- 8 F. Carn, A. Colin, O. Pitois and R. Backov, *Soft Matter*, 2012, **8**, 61–65.
- 9 S. Guignot, S. Faure, M. Vignes-Adler and O. Pitois, *Chemical Engineering Science*, 2010, **65**, 2579–2585.
- 10 I. Lesov, S. Tcholakova and N. Denkov, *Journal of colloid and interface science*, 2014, **426**, 9–21.
- 11 I. Lesov, S. Tcholakova and N. Denkov, *RSC Advances*, 2014, **4**, 811–823.
- 12 J. Goyon, F. Bertrand, O. Pitois and G. Ovarlez, *Physical Review Letters*, 2010, **104**, 128301.
- 13 A. Salonen, R. Lhermerout, E. Rio, D. Langevin and A. Saint-Jalmes, *Soft Matter*, 2012, **8**, 699–706.
- 14 B. Haffner, Y. Khidas and O. Pitois, *Soft matter*, 2014, **10**, 3277–3283.
- 15 Y. Khidas, B. Haffner and O. Pitois, *Soft matter*, 2014, **10**, 4137–4141.
- 16 F. Rouyer, B. Haffner, N. Louvet, Y. Khidas and O. Pitois, *Soft Matter*, 2014, **10**, 6990–6998.
- 17 B. Haffner, Y. Khidas and O. Pitois, *Journal of Colloid and Interface Science*, 2015, **458**, 200–208.
- 18 S. Cohen-Addad, M. Krzan, R. Höhler and B. Herzhaft, *Physical Review Letters*, 2007, **99**, 168001.
- 19 J. Wang, A. V. Nguyen and S. Farrokhpay, *Advances in Colloid and Interface Science*, 2016, **228**, 55–70.
- 20 A. Cervantes Martinez, E. Rio, G. Delon, A. Saint-Jalmes, D. Langevin and B. P. Binks, *Soft Matter*, 2008, **4**, 1531.
- 21 J. Wang and A. V. Nguyen, *Soft Matter*, 2016, **12**, 3004–3012.
- 22 F. Gorlier, Y. Khidas, A. Fall and O. Pitois, *Physical Review E - Statistical, Nonlinear, and Soft Matter Physics*, 2017, **95**, 42604.
- 23 F. Gorlier, Y. Khidas and O. Pitois, *Journal of Colloid And Interface Science*, 2017, **501**, 103–111.
- 24 A. Nguyen and H. J. Schulze, *Colloidal Science of Flotation*, Marcel Dekker, New York, 2003.
- 25 D. Turner, B. Dlugogorski and T. Palmer, *Colloids and Surfaces A: Physicochemical and Engineering Aspects*, 1999, **150**, 171–184.
- 26 M. Kogan, L. Ducloué, J. Goyon, X. Chateau, O. Pitois and G. Ovarlez, *Rheologica Acta*, 2013, **52**, 237–253.
- 27 L. Ducloué, O. Pitois, J. Goyon, X. Chateau and G. Ovarlez, *Soft matter*, 2014, **10**, 5093–8.

- 28 L. Ducloué, O. Pitois, J. Goyon, X. Chateau and G. Ovarlez, *Journal of Non-Newtonian Fluid Mechanics*, 2015, **215**, 31–39.
- 29 L. Ducloué, O. Pitois, L. Tocquer, J. Goyon and G. Ovarlez, *Colloids and Surfaces A: Physicochemical and Engineering Aspects*, 2017, **513**, 87–94.
- 30 A. Ö. Özarmut and H. Steeb, *Journal of Physics: Conference Series*, 2015, **602**, 12031.
- 31 F. G. Gandolfo and H. L. Rosano, *Journal of colloid and interface science*, 1997, **194**, 31–36.
- 32 I. Cantat, S. Cohen-Addad, F. Elias, F. Graner, R. Höhler, O. Pitois and F. Rouyer, *Foams: Structure and Dynamics*, Oxford University Press, Oxford, 2013.
- 33 L. J. Gibson and M. F. Ashby, *Cellular Solids: Structure and Properties*, Cambridge University Press, Cambridge, 1997.
- 34 I. Cantat and O. Pitois, *Physics of Fluids*, 2006, **18**, 83302.
- 35 I. Cantat and O. Pitois, *Journal of Physics: Condensed Matter*, 2005, **17**, S3455–S3461.
- 36 F. Mahaut, F. Bertrand, P. Coussot, X. Chateau and G. Ovarlez, *AIP Conference Proceedings*, 2008, **1027**, 671–673.
- 37 Y. Khidas, B. Haffner and O. Pitois, *Composites Science and Technology*, 2015, **119**, 62–67.
- 38 N. Louvet, R. Höhler and O. Pitois, *Physical Review E*, 2010, **82**, 41405.

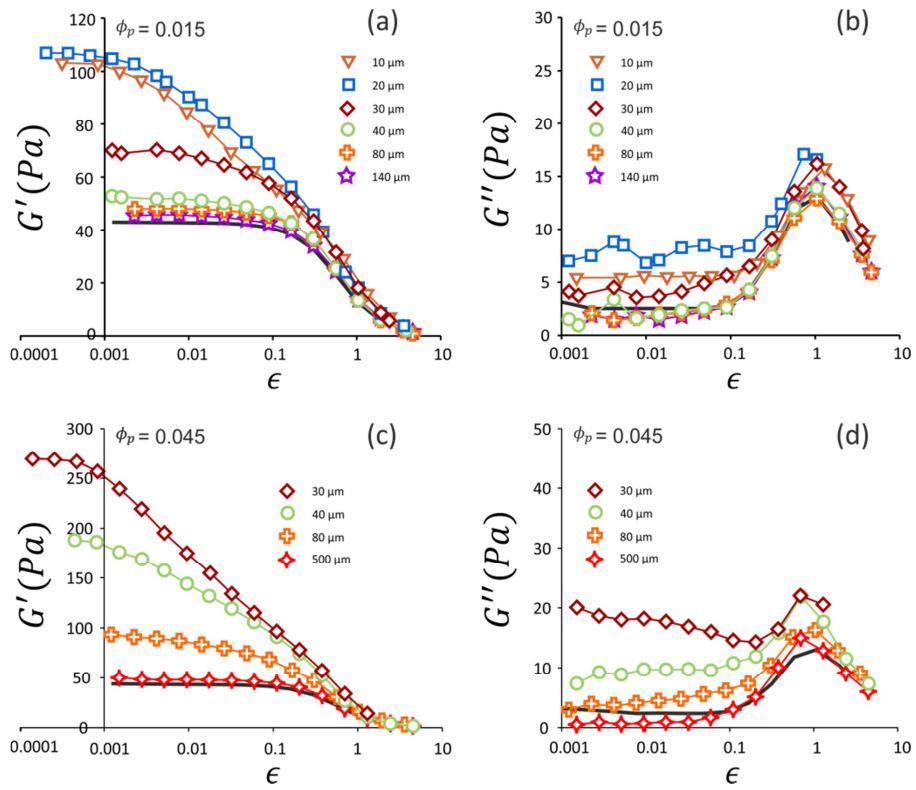


Fig. 1: (a,c) Shear elastic modulus  $G'$  and (b,d) shear loss modulus  $G''$  as a function of strain amplitude (imposed at a frequency equal to 1 Hz) for aqueous foams loaded with particles of different diameters. Two particle volume fractions are presented:  $\phi_p = 0.015$  (a,b) and 0.045 (c,d). Solid lines represent the particle-free foam.

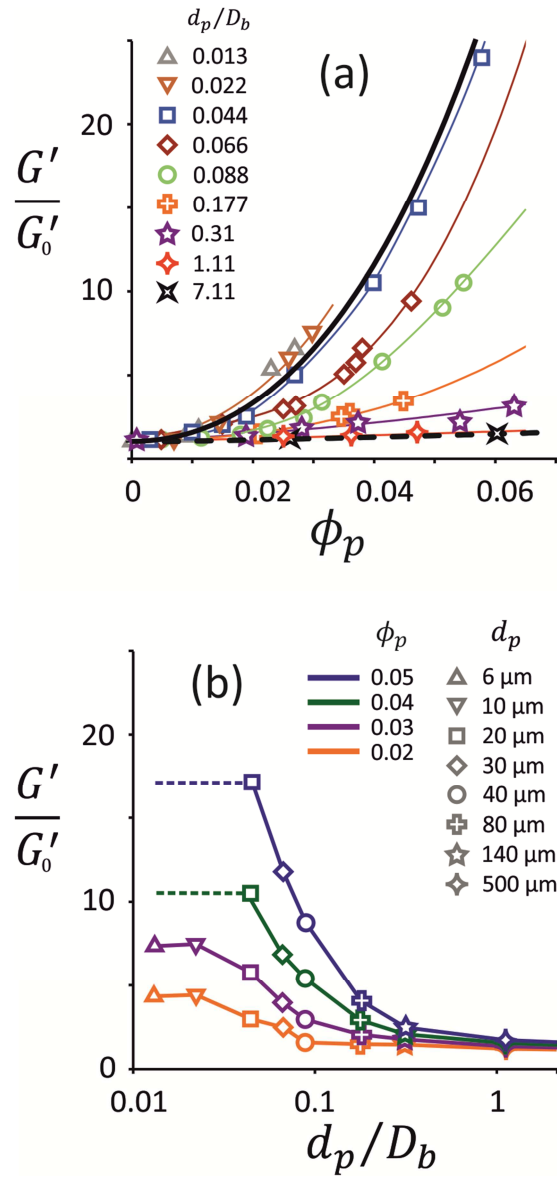


Fig. 2: (a) Reduced elastic modulus  $G'/G'_0$  measured as a function of the particle volume fraction for several particle-to-bubble size ratios. Continuous and dashed black lines correspond to eqs 1 and 2 respectively. (b) Reduced elastic modulus  $G'/G'_0$  as a function of particle-to-bubble size ratio for several particle volume fractions  $\phi_p$  and several particle sizes  $d_p$ . Note that several points have been obtained from interpolation and extrapolation of experimental data presented in 2a.

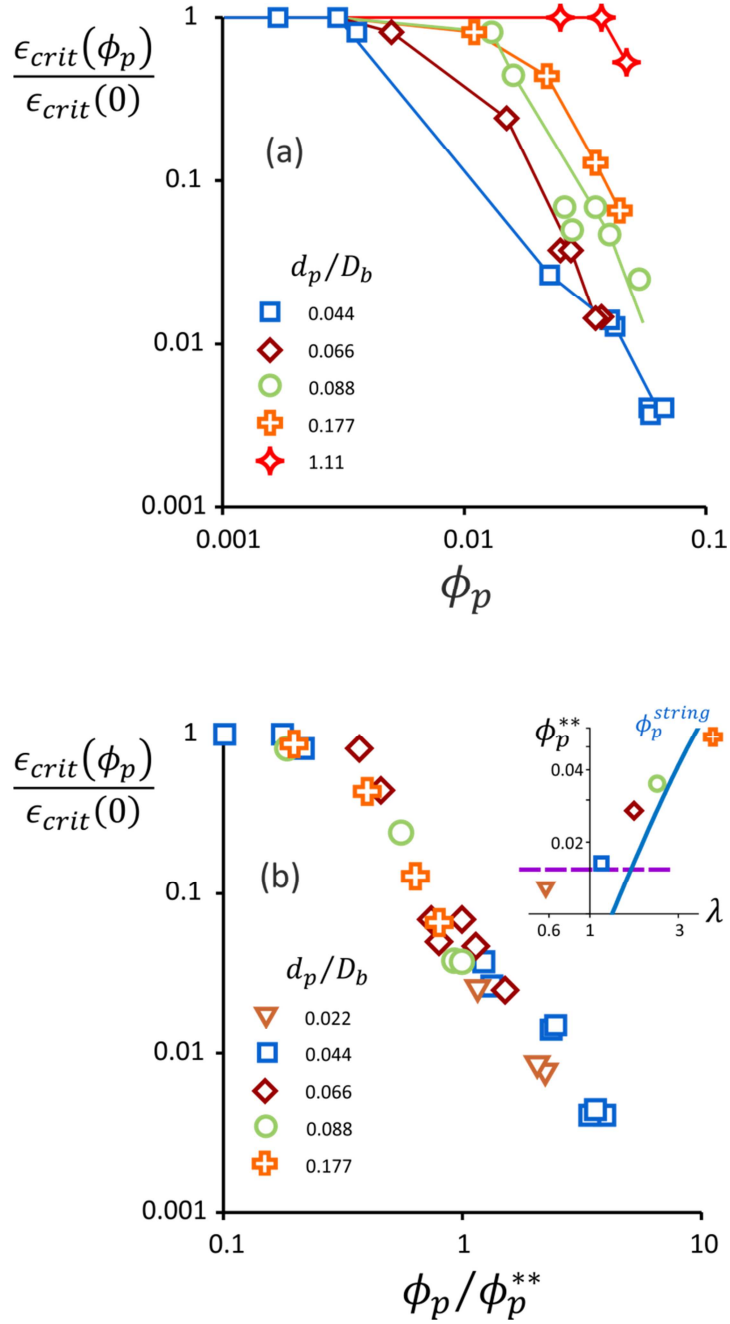


Fig. 3: (a) Reduced critical strain amplitude  $\epsilon_{crit}(\phi_p)/\epsilon_{crit}(0)$  as a function of the particle volume fraction for several particle-to-bubble size ratios. (b) Reduced critical strain amplitude  $\epsilon_{crit}(\phi_p)/\epsilon_{crit}(0)$  as a function of reduced particle volume fractions  $\phi_p/\phi_p^{**}$  (see details about  $\phi_p^{**}$  in the main text) for several particle-to-bubble size ratios. Inset: characteristic particle volume fraction  $\phi_p^{**}$  as a function of the confinement parameter  $\lambda$ . The continuous line corresponds to eq. 4.

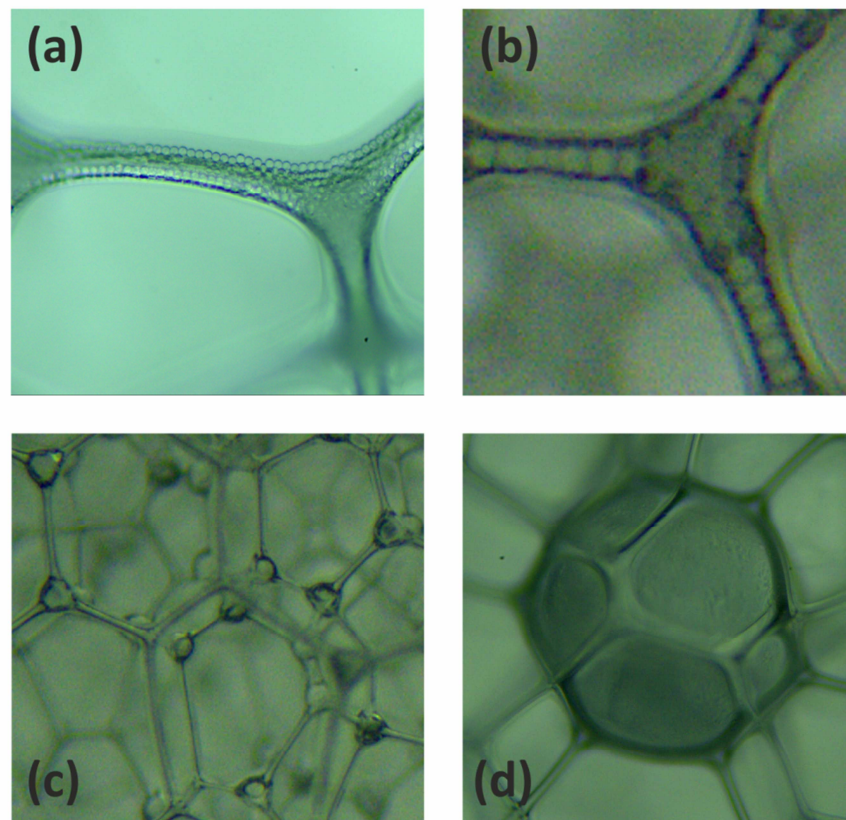


Fig. 4: Images of particle-loaded foams showing the evolution of the microstructure as particle size increases (bubble size is equal to  $450\ \mu\text{m}$ ; length scale is given by the particle size indicated in the following). (a) packings of particles ( $d_p = 10\ \mu\text{m}$ ,  $\phi_p \approx 1.5\%$ ), (b) strings of particles ( $d_p = 40\ \mu\text{m}$ ,  $\phi_p \approx 2.5\%$ ), (c) isolated particles in foam nodes ( $d_p = 80\ \mu\text{m}$ ,  $\phi_p \approx 1\%$ ), (d) isolated large particles embedded in foam ( $d_p = 500\ \mu\text{m}$ ,  $\phi_p \approx 3\%$ ).

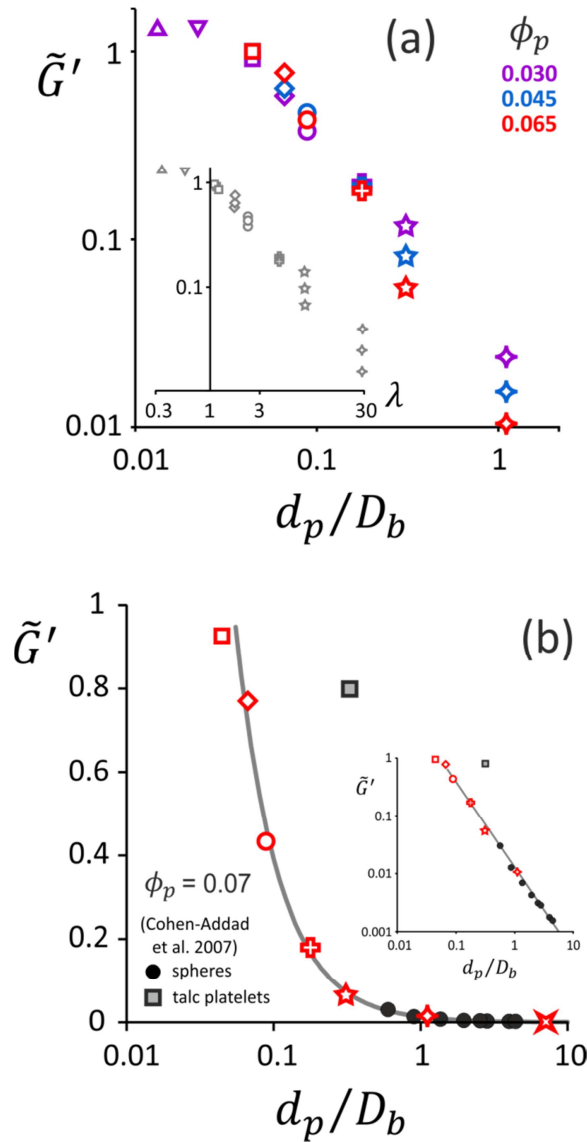


Fig. 5: (a) Normalized elastic modulus  $\tilde{G}'$  defined by eq. 3 as a function of particle-to-bubble size ratio for several particle volume fractions. Inset: Normalized elastic modulus  $\tilde{G}'$  as a function of the confinement parameter  $\lambda$ . (b) Normalized elastic modulus  $\tilde{G}'$  defined by eq. 3 as a function of particle-to-bubble size ratio for a particle volume fraction  $\phi_p \approx 0.07$ . Empty symbols represent data of figure 5a ( $\phi_p = 0.065$ ) and filled symbols represent data from reference <sup>18</sup> and adapted according to eq. 3 (see main text for details). Note that filled circles represent spherical particles whereas the filled square represents plate-like talc particles. Grey line is a power law:  $\tilde{G}' = 0.013(d_p/D_b)^{-1.48}$ . Inset: Normalized elastic modulus  $\tilde{G}'$  as a function of particle-to-bubble size ratio.

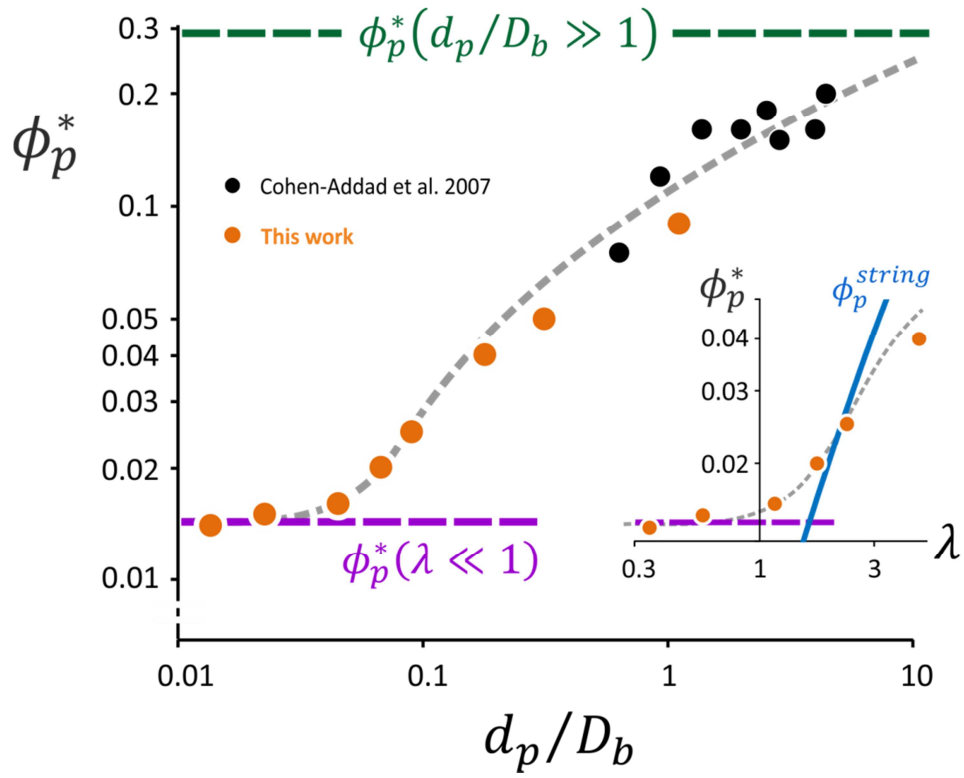


Fig. 6: Characteristic particle volume fraction  $\phi_p^*$  as a function of particle-to-bubble size ratio. The dashed grey line is a guide for the eye. Thick horizontal dashed lines represent the particle volume fractions discussed in the main text. Inset: Characteristic particle volume fraction  $\phi_p^*$  as a function of the confinement parameter  $\lambda$ . The continuous line corresponds to eq. 4.